Research Square

Preprints are preliminary reports that have not undergone peer review.
They should not be considered conclusive, used to inform clinical practice,
or referenced by the media as validated information.

Systematic Surface Modification of Hydrated Silica for Enhanced Flavourzyme Immobilization: Toward Cleaner and Reusable Biocatalysis in Food Processing

Xu Zhao
South China University of Technology
Yuqin Cheng
South China University of Technology
Lei Cai
Gannan Medical University
Chun Cui
cuichun@scut.edu.cn

South China University of Technology

Research Article

Keywords: Flavourzyme, Immobilization, Hydrated silica, Surface modification, Catalytic stability, Reusability

Posted Date: May 25th, 2026

DOI: https://doi.org/10.21203/rs.3.rs-9640406/v1

License: This work is licensed under a Creative Commons Attribution 4.0 International License.
Read Full License

Additional Declarations: No competing interests reported.

Abstract

Enzyme immobilization offers a promising strategy to enhance biocatalyst stability, reusability, and operational performance in industrial bioprocesses. In this study, hydrated silica (HS) was surface-engineered via four distinct chemistries—amination (AHS), carboxylation (CHS), polydopamine coating (DHS), and epoxidation (EHS)—to develop robust carriers for Flavourzyme immobilization. The modified supports were characterized by diffuse reflectance Fourier-transform infrared spectroscopy (DR-FTIR) and X-ray photoelectron spectroscopy (XPS), confirming successful functionalization. Immobilization conditions were optimized for each system through single-factor experiments. Among the carriers, DHS achieved the best overall performance with 42.02% immobilization rate and 73.69% enzyme activity recovery. Compared to free Flavourzyme, immobilized systems demonstrated enhanced pH and thermal stability, broader operational ranges, and superior reusability. DHS-F retained over 50% activity after 20 cycles and exhibited excellent storage stability. Principal component analysis (PCA) identified storage stability and reusability as the key discriminators among immobilized systems. These findings demonstrate that surface-engineered HS, especially DHS, provides a scalable and recyclable platform for stable Flavourzyme immobilization, with potential for continuous operation in food protein hydrolysis processes, supporting sustainable and resource-efficient biocatalytic processes.

1. Introduction

Enzymes are exceptional biocatalysts capable of significantly reducing the energy demand of biochemical reactions while enhancing conversion efficiency (Guisan et al. 2022). In industrial biotechnology, enzymes have been increasingly integrated across tdiverse production chains—from raw material processing to product quality improvement (Haghighat-Kharazi et al. 2020; Mao et al. 2024). For instance, amylase facilitates starch hydrolysis during biofuel and biochemical production (Chen et al. 2021), pectinase is widely used to clarify plant extracts (Patel et al. 2022), and β-galactosidase effectively hydrolyzes lactose into galactose and glucose for dairy application (Nowak et al. 2021). Despite their widespread application, the industrial use of free enzymes faces several challenges. High production costs, poor operational stability under processing conditions (e.g., elevated temperature or extreme pH), and difficulties in recovery and reuse hinder their large-scale adoption (Yang et al. 2023). These limitations underscore the need for robust enzyme delivery systems that can maintain catalytic activity while enhancing stability and recyclability (Bhatia et al. 2023).

Enzyme immobilization has emerged as a key strategy to address these challenges (Tadesse and Liu 2025). By anchoring enzymes onto solid supports or confining them within matrices, immobilization can significantly improve enzyme stability, facilitate separation, and enable repeated use—thereby enhancing the economic and environmental sustainability of biocatalytic processes (Maghraby et al. 2023). Among various immobilization techniques, covalent binding is particularly attractive due to its strong enzyme–carrier interactions, which minimize enzyme leaching and improve operational durability (Mohamad et al. 2015; Wiltschi et al. 2020). The performance of immobilized enzymes is heavily influenced by the physicochemical properties of the support material. Hydrated silica (HS) has gained attention as an

enzyme carrier due to its high surface area, excellent mechanical stability, and ease of surface functionalization (Zdarta et al. 2018). However, pristine silica surfaces often lack sufficient reactive groups for efficient enzyme binding (Ashkan et al. 2021). To overcome this, surface modification is essential to introduce functional groups (e.g., amino, carboxyl, epoxy, or catechol) that can facilitate strong and selective enzyme attachment.

Flavourzyme, a commercial protease complex produced by *Aspergillus oryzae*, is widely used in industrial biotechnology for protein hydrolysis and biocatalytic applications. It plays a key role in improving the solubility and digestibility of protein-based substrates (Yang et al. 2020). Beyond generic proteolysis, Flavourzyme has been successfully employed in several industrial segments, including cheese ripening acceleration (Gao et al. 2022), plant protein modification (Shuai et al. 2022; Grossmann et al. 2021; Li et al. 2025), and meat tenderization (Zhang et al. 2017; Feng et al. 2014). Despite these benefits, free Flavourzyme is supplied as a liquid concentrate that is fully discharged after each batch; it cannot be economically recovered by centrifugation or membrane separation. This single-use pattern results in high enzyme costs and a significant effluent chemical oxygen demand (COD) load, making multi-cycle operation economically and environmentally unattractive (Zhao et al. 2025; Katic et al. 2021).

In this study, we systematically investigated the surface modification of hydrated silica using four distinct chemical strategies—amination, carboxylation, polydopamine coating, and epoxidation—to develop tailored carriers for Flavourzyme immobilization. The modified supports were thoroughly characterized by DR-FTIR and XPS, and the immobilization process was optimized for each system via single-factor experiments. The resulting biocatalysts were evaluated in terms of immobilization efficiency, catalytic performance, pH and thermal stability, storage stability, and reusability. Furthermore, principal component analysis (PCA) was employed to comprehensively assess and compare the performance of different immobilized systems. This work aims to establish a robust, efficient, and reusable Flavourzyme immobilization platform based on surface-engineered hydrated silica, contributing to cleaner and more sustainable biocatalytic processes in the food industry.

2. Materials and Methods

2.1 Materials

Hydrated silica was kindly supplied by Evonik Degussa (China) Investment Co., Ltd. Glutaraldehyde, ethylenediamine, 6-aminocaproic acid, dopamine hydrochloride, and epichlorohydrin were purchased from Shanghai Macklin Biochemical Technology Co., Ltd. Flavourzyme® 1000L (produced by *Aspergillus oryzae*) was donated by Novozymes (China) Biotechnology Co., Ltd. All other reagents used in this study were of analytical grade.

2.2 Surface modification of hydrated silica (HS)

Prior to modification, hydrated silica (HS, 10 g) was washed three times with de-ionised water (3 × 100 mL), soaked in absolute ethanol (100 mL, 24 h) to remove organic contaminants, rinsed again with water

(2 × 100 mL) and dried under vacuum at 60°C for 12 h and stored in a desiccator. Silica was first activated with glutaraldehyde (common step), then subjected to four parallel functionalization routes. (i) GA activation: dry HS (1.0 g) was suspended in 5 wt % aqueous glutaraldehyde (10 mL) and shaken (200 rpm) at 37°C for 4 h. The solid was recovered by vacuum filtration, washed with water (3 × 20 mL) and vacuum-dried (40°C, 6 h). (ii) Amination (AHS): the activated support was reacted with 3 wt % ethylenediamine (10 mL) at 30°C and 200 rpm for 8 h (Gennari et al. 2018). After filtration the product was washed to neutral pH and dried under vacuum (40°C, 6 h). (iii) Carboxylation (CHS): the activated support was treated with 8 wt % 6-aminocaproic acid (10 mL) at 60°C and 200 rpm for 4 h (Li et al. 2020), work-up followed the procedure described for AHS. (iv) Dopamine coating (DHS): activated HS was immersed in 2 mg/mL dopamine hydrochloride solution (10 mL, 0.1 M Tris-HCl, pH 8.5) and shaken (200 rpm) at 25°C for 12 h (Zheng et al. 2021). The slurry was filtered, rinsed sequentially with ethanol (20 mL) and water (3 × 20 mL) until the filtrate was colorless, and vacuum-dried (40°C, 6 h). (v) Epoxidation (EHS): dried HS (1.0 g) was dispersed in 1 M NaOH (10 mL); epichlorohydrin (15% v/v, 45 mL) and an equal volume of DMSO (45 mL) were added. The mixture was shaken (200 rpm) at 50°C for 3 h (Johansson et al. 2003). The solid was recovered by filtration, washed with ethanol (2 × 30 mL) and water (3 × 30 mL), and vacuum-dried (40°C, 6 h). Functionalized silicas were denoted as AHS (amino), CHS (carboxyl), DHS (dopamine) and EHS (epoxy) and stored in a desiccator until further use.

2.3 Diffuse Reflectance Fourier Transform Infrared Spectroscopy (DR-FTIR)

Spectra were acquired on a Nicolet 6700 FT-IR spectrometer (Thermo Fisher, USA) equipped with a Praying Mantis™ diffuse-reflectance accessory. Samples (~ 2 wt %) were gently ground with spectroscopic-grade KBr and pressed into 13 mm pellets. All spectra were recorded over 4 000–400 cm^{-1} at 4 cm^{-1} resolution; 64 scans were co-added and averaged to improve the signal-to-noise ratio. Background correction was performed against pure KBr measured under identical conditions.

2.4 X-ray photoelectron spectroscopy (XPS)

XPS analysis was carried out with a K-Alpha™ spectrometer (Thermo Fisher, UK) using monochromated Al Kα radiation (hv = 1 486.6 eV) operated at 12 kV and 3 mA. Survey spectra (0–1 350 eV) were collected at a pass energy of 200 eV, while high-resolution C 1s, O 1s, N 1s and Si 2p regions were recorded at 50 eV pass energy with a 0.1 eV step. The analysis spot diameter was 400 µm and the take-off angle 90°. Charge compensation was achieved with a low-energy electron flood gun; binding energies were calibrated to the adventitious C 1s peak at 284.8 eV. Spectral deconvolution and quantification were performed using Avantage v. 5.992 and XPSPEAK 4.1 software with Shirley background subtraction and a 70% Gaussian / 30% Lorentzian line-shape. Atomic concentrations were calculated from peak areas using the instrument-specific sensitivity factors provided by the manufacturer.

2.5 Immobilization of Flavourzyme

Modified hydrated-silica carriers (AHS, CHS, DHS or EHS) were first equilibrated in 0.1 M potassium phosphate buffer (PBS, pH 7.0) for 30 min and recovered by vacuum filtration. For each carrier, enzyme

solution (2–10 mg protein mL^{-1}, 10 mL, 0.1 M PBS) was prepared by diluting Flavourzyme® 1000 L with the same buffer. The solid-to-liquid ratio was varied from 1:1 to 1:15 (w/v, dry basis) by adjusting the mass of carrier while keeping the liquid volume constant at 10 mL. The suspension was shaken (200 rpm) in a thermostatic incubator over 4–20 h; temperature (25–55°C) and pH (5.0–9.0) were varied systematically according to a one-factor-at-a-time (OFAT) protocol established from preliminary trials. After the chosen interval, the solid was separated by filtration (0.45 μm nylon membrane), rinsed with 3 × 10 mL of fresh buffer to remove loosely bound protein, blotted on filter paper and dried under vacuum (25°C, 6 h). The resulting immobilized enzymes were stored at 4°C and used within 48 h. The filtrate and combined washings were retained for BCA protein assay and activity measurement, allowing calculation of immobilization rate and enzyme activity recovery. Carriers are hereafter denoted AHS-F, CHS-F, DHS-F and EHS-F, respectively.

2.6 Determination of immobilization rate

The protein concentration in the combined filtrate and washings was determined with a BCA Protein Assay Kit (Thermo Fisher, USA) using bovine serum albumin as standard. The immobilization rate was calculated as:

$$\text{Immobilization rate (\%)} = \frac{C_0 \times V_0 - C_t \times V_t}{C_0 \times V_0} \times 100\%$$

where C_0 and C_t are the protein contents (mg/mL) and V_0 and V_t are the total volumes (mL) of the liquid phase before and after immobilization, respectively.

2.7 Determination of enzyme activity recovery

The enzyme activity of the immobilized Flavourzyme was measured by the Folin-Ciocalteu method using casein as substrate. One unit (U) is defined as the amount of enzyme that liberates 1 μg of tyrosine per minute at 40°C and pH 7.5. The enzyme activity recovery was calculated as:

$$\text{Enzyme activity recovery (\%)} = \frac{\text{Total immobilized enzyme activity (U)}}{\text{Total free enzyme activity (U)}} \times 100\%$$

2.8 Catalytic properties of immobilized Flavourzyme

The optimum pH was determined by incubating free or immobilized Flavourzyme at 25°C for 10 min in 0.1 M buffers covering pH 4.0–10.0 (citrate 4.0–5.5, phosphate 6.0–8.0, glycine-NaOH 8.5–10.0). Temperature profiling was carried out at 25–70°C. Proteolytic activity was measured in triplicate by the Folin-Ciocalteu casein assay; results are expressed as relative activity (%) with the maximum set to 100%.

2.9 pH and thermal stability of immobilized Flavourzyme

Free or immobilized Flavourzyme was incubated at 25°C for 10 h in 0.1 M buffers (pH 4–10). Residual activity was then measured under optimal conditions and expressed as percentage of the untreated control (100%). For thermal stability, aliquots were kept at 25, 35, 45, 55, 65 and 75°C (pH 7.5, 10 h), cooled on ice and assayed in triplicate; residual activity was calculated relative to the unheated control.

2.10 Storage stability of immobilized Flavourzyme

Free and immobilized Flavourzyme were stored in 0.1 M PBS (pH 7.5) at 4°C without any preservative. At 5-day intervals over 30 days, aliquots were withdrawn in triplicate and assayed under optimal conditions. Residual activity is reported relative to the initial value (day 0 = 100%).

2.11 Reusability of immobilized Flavourzyme

The same immobilized preparation (10 mg dry weight) was subjected to 20 successive hydrolysis cycles. Each cycle consisted of 30 min hydrolysis of 1% (w/v) casein in 0.1 M phosphate buffer (pH 7.5, 40°C) followed by rapid filtration, three washes with buffer, and immediate re-use. Activity was measured at the end of every cycle and expressed relative to the first cycle (100%). All measurements were performed in triplicate.

2.12 Principal component analysis (PCA)

PCA was performed using SPSS 20.0 (SPSS Inc., Chicago, IL, USA) to analyze the multivariate dataset comprising immobilization rate, enzyme activity recovery, optimal pH/temperature, pH- and thermal-stability, storage stability at 10, 30, and 50 d, and reusability after 10 and 20 cycles. Variables were standardized (z-score normalization) prior to analysis to ensure equal weighting.

2.13 Statistical Analysis

All determinations were carried out in independent triplicates and are reported as mean ± standard deviation. One-way analysis of variance (ANOVA) followed by Duncan's multiple-range test (SPSS 20.0, SPSS Inc., Chicago, IL, USA) was used to assess differences among groups; $p < 0.05$ was considered statistically significant.

3. Results and Discussion

3.1 DR-FTIR analysis of modified hydrated silica (HS)

The DR-FTIR spectra in Fig. 1 provide insights into the chemical structures of the modified HS. For AHS (Fig. 1A), the appearance of characteristic peaks at 1296–1332 cm^{-1}, corresponding to C-N bond stretching vibrations, confirms the successful grafting of ethylenediamine onto the HS surface (De Meutter and Goormaghtigh 2021). The peak at 2933 cm^{-1} is attributed to the stretching vibration of the N-H bonds, while the absorption peak at 1645 cm^{-1} is assigned to the in-plane bending vibration of the N-H bonds in -NH_2 groups. These typical absorption peaks of amino groups in ethylenediamine validate the formation of an aminated structure on the HS surface (Intarabumrung et al. 2022). The DR-FTIR

spectrum of CHS (Fig. 1B) exhibits strong absorption bands between 1217–1653 cm^{-1} associated with the stretching vibrations of C-N and C-O bonds. This indicates covalent bonding between aminocaproic acid and aldehyde groups on HS surface via a condensation reaction (Zhao et al. 2005). Peaks between 1300–1450 cm^{-1} are likely due to the symmetric stretching vibrations of COO^- in carboxylates, suggesting that some aminocaproic acid may exist in ionic form on the HS surface (Benke et al. 1998; Daulay et al. 2024). DHS (Fig. 1C) shows characteristic peaks between 1450–1546 cm^{-1}, attributed to the stretching vibrations of C = C bonds in the aromatic rings of polydopamine. The absorption band between 1220–1700 cm^{-1} corresponds to the stretching vibrations of C-N bonds (Guo et al. 2023), with the peak at 1454 cm^{-1} assigned to the bending vibration of -NH- bonds and the vibration of $-NH_2$ bonds appearing at 1662 cm^{-1}. These results are consistent with previous studies, confirming that dopamine underwent oxidative self-polymerization on the HS surface to form a polydopamine coating (Eshaghi and Pouransari 2025). For EHS (Fig. 1D), a characteristic peak is observed at 1676 cm^{-1}, attributed to the stretching vibration of C = O bonds. The stretching vibrations of C-O bonds occur between 1183–1331 cm^{-1}, aligning with prior findings (Daulay et al. 2024). This indicates that the ring-opening reaction of epichlorohydrin with hydroxyl groups on the HS surface formed new C-O bonds. Additionally, the absorption band between 2900–3055 cm^{-1} corresponds to the stretching vibrations of saturated C-H bonds, and the absorption peak at 781 cm^{-1} is attributed to the carbon-chlorine bond, confirming the successful introduction of the alkyl chain of epichlorohydrin onto the HS surface (Talik et al. 2020).

3.2 XPS analysis

High-resolution XPS spectra (Fig. 2) and surface atomic compositions (Table 1) confirm successful functionalization. Pristine HS exhibits the expected SiO_2 signature (Si 2p = 103.2 eV, O 1s = 532.9 eV) with low adventitious carbon (7.35 at %) (Laguri et al. 2018). After modification, nitrogen is detected on AHS (4.54 at %), DHS (6.18 at %) and CHS (0.6 at %), while oxygen increases from 40.5 to 70.3 at % (CHS) and 71.8 at % (EHS), consistent with the introduced O-containing linkers. Deconvolution of the C 1s envelopes reveals the anticipated chemical shifts: AHS exhibits contributions from C–N/C–OH at 285.8 eV along with a shoulder peak at 286.2 eV that can be attributed to the C = N double bond of imines, corroborating Schiff-base coupling of ethylenediamine (Das et al. 2022; Tan et al. 2023). The N 1s spectrum further exhibits two peaks corresponding to primary/secondary amines at 399.5 eV and tertiary amines at 401.4 eV, confirming the successful grafting of ethylenediamine and the formation of aminated structure on the HS surface (Huang et al. 2018). CHS exhibits a carboxyl C = O component at 287.1 eV and COO^- satellites at 530.4–531.8 eV in the O 1s region, verifying 6-aminocaproic acid anchoring (Tang et al. 2019; Fujisaki et al. 2024). DHS displays catechol/quinone O 1s peaks at 531.5 eV and 532.9 eV together with C = N (403.4 eV) in the N 1s spectrum, consistent with polydopamine film formation (Jiang et al. 2010; Chao et al. 2014; Atrei et al. 2024). EHS presents C–O–C (285.9 eV) and O–C = O (288.1 eV) carbon environments together with residual epoxy signals (531.5 eV and 532.9 eV), confirming ring-opening of epichlorohydrin and grafting of the alkyl chain (Li et al. 2018; Shen et al. 2018). Thus, each modification route introduces the expected surface functionalities, providing a versatile platform for subsequent enzyme immobilization.

Table 1
Surface elemental compositions of pristine and functionalized hydrated silica (HS, pristine hydrated silica; AHS, amino-modified hydrated silica; CHS, carboxyl-modified hydrated silica; DHS, dopamine-modified hydrated silica; EHS, epoxy-modified hydrated silica)

Elemental compositions (at %)	HS	CHS	DHS	AHS	EHS
C	7.35	20.34	16.55	39.48	18.4
N	0	0.6	6.18	4.54	0
O	40.49	70.25	56.93	35.53	71.84
Si	52.54	8.81	20.34	20.44	9.64

3.3 Optimization of immobilization conditions for modified HS

3.3.1 Optimization of AHS-F immobilization conditions

The immobilization behavior of Flavourzyme on AHS was systematically optimized with respect to enzyme concentration, temperature, pH, reaction time, and solid-to-liquid ratio. At low enzyme loadings, immobilization efficiency increased linearly with concentration due to the availability of free amino groups on the carrier. Saturation was reached at 6 mg/mL, beyond which no further increase in loading was observed (Fig. 3AHS-a). However, enzyme activity recovery plateaued at 11.95%, suggesting that overcrowding of enzyme molecules restricted substrate accessibility (Carballares et al. 2022). Thus, 6 mg/mL was selected as the optimal enzyme concentration. Temperature exerted a dual effect: while higher temperatures enhanced collision frequency, they also promoted protein denaturation (Flores et al. 2019). At 50°C, although the immobilization rate reached 80%, enzyme activity recovery dropped sharply to 5%. In contrast, 25°C balanced both metrics, yielding 62.33% immobilization and 26.51% enzyme activity recovery (Fig. 3AHS-b). pH influenced both enzyme stability and carrier–enzyme electrostatic interactions (Dotsenko et al. 2024). Immobilization rate peaked at pH 8, but enzyme activity recovery collapsed (> 90% loss). At pH 6, immobilization rate was moderate (50%), but enzyme activity recovery was maximized (23.83%) (Fig. 3AHS-c). Hence, pH 6 was chosen. Prolonged reaction times led to enzyme desorption and deactivation. A 4 h window provided the best compromise: 60% immobilization rate and 40% enzyme activity recovery (Fig. 3AHS-d). Finally, the solid-to-liquid ratio governed enzyme–carrier contact probability (Li et al. 2024). A 1:10 ratio maximized both immobilization rate (64.03%) and enzyme activity recovery (39.70%) (Fig. 3AHS-e).

3.3.2 Optimization of CHS-F immobilization conditions

For CHS-F, enzyme concentration was optimized first. Enzyme activity recovery increased with loading up to 8 mg/mL, reaching 57.09%, while immobilization rate plateaued at 43.15% (Fig. 3CHS-a). Beyond this point, steric hindrance and mass-transfer limitations reduced enzyme activity recovery (Bolivar and Nidetzky 2019); thus, 8 mg/mL was selected. Temperature screening revealed that enzyme activity

recovery declined monotonically with increasing temperature, whereas immobilization rate peaked at 35°C (Fig. 3CHS-b). Elevated temperatures weakened the Schiff-base linkages, promoting enzyme leaching (Saroja and Bhat 2021). Consequently, 25°C was adopted. pH optimization showed a maximum in both immobilization rate and enzyme activity recovery at pH 8 (Fig. 3CHS-c). Reaction time profiling indicated that 12 h was required to reach equilibrium (Fig. 3CHS-d). Finally, a 1:15 solid-to-liquid ratio offered the best trade-off between cost and performance: 63.56% immobilization rate and 71.95% enzyme activity recovery (Fig. 3CHS-e).

3.3.3 Optimization of DHS-F immobilization conditions

DHS-F exhibited similar trends to CHS-F. Enzyme saturation occurred at 8 mg/mL, with enzyme activity recovery and immobilization rate at 57.09% and 39.44%, respectively (Fig. 3DHS-a). Higher loadings caused a decline in both metrics. Temperature and pH optima were 25°C and pH 7, respectively (Fig. 3DHS-b,c). Reaction time and solid-to-liquid ratio optima were identical to CHS-F: 12 h and 1:15 (Fig. 3DHS-d,e). Final results achieved a 42.02% immobilization rate and 73.69% enzyme activity recovery.

3.3.4 Optimization of EHS-F immobilization conditions

EHS-F displayed distinct behavior. Immobilization rate decreased with enzyme concentration, whereas enzyme activity recovery increased up to 6 mg/mL and then plateaued (~ 38%) (Fig. 3EHS-a). Low loadings favored full utilization of active sites; higher loadings induced competitive binding. Thus, 6 mg/mL was selected. Temperature screening showed a maximum in both metrics at 25–35°C (Fig. 3EHS-b). Above 35°C, experienced a significant drop, approaching zero at 50°C due to thermal denaturation. Therefore, 25°C was considered optimal for balancing both immobilization rate and enzyme activity recovery. pH profiling revealed that immobilization rate peaked at pH 8, while enzyme activity recovery was highest at pH 6 (Fig. 3EHS-c). To balance both, pH 6 was adopted. Reaction time optimization indicated that enzyme activity recovery declined after 4 h, whereas immobilization rate peaked at 16 h (Fig. 3EHS-d). Prioritizing catalytic performance, 4 h was selected. A 1:10 solid-to-liquid ratio maximized enzyme activity recovery (44.68%) while maintaining acceptable immobilization rate (52.92%) (Fig. 3EHS-e).

3.4 Optimal catalytic pH and temperature of immobilized Flavourzyme

Compared with the free Flavourzyme (FF), all immobilized preparations exhibited a pronounced alkaline shift in their optimal pH (Fig. 4A). FF displayed maximum activity at pH 7, whereas AHS-F and DHS-F moved the optimum to pH 8. CHS-F and EHS-F produced an even stronger displacement (optimum pH 9). The micro-environment created by the charged or H-bonding groups on the carrier stabilizes the protonation state of key residues, delaying denaturation under alkaline conditions (Yang et al. 2017).

The temperature optimum was also carrier-dependent (Fig. 4B). FF retained maximal activity at 50°C, whereas CHS-F and DHS-F peaked at 60°C, indicating that covalent cross-linking rigidifies the active site

and suppresses heat-induced unfolding. AHS-F, in contrast, gave its highest activity at 40°C, suggesting that electrostatic interactions with the amino-functionalized surface slightly perturb enzyme conformation and reduce thermal tolerance (Cai et al. 2025). EHS-F showed a peak activity at 50°C, similar to FF, but with a broader activity range extending up to 70°C. CHS-F and DHS-F preserved > 60% of their maximum activity between 40 and 70°C, whereas FF lost > 50% of its activity above 60°C. These results agree with previous reports of nanoparticle-immobilized lipases that gained 5–10°C thermal tolerance after covalent attachment (Nasiri et al. 2025), confirming that immobilization broadens the operational temperature window of Flavourzyme.

3.5 pH and thermal stability of immobilized Flavourzyme

The pH stability of both free and immobilized Flavourzyme was evaluated after a 10-hour incubation at 25°C across a pH range from 4 to 10, as shown in Fig. 5A. FF showed significant variation in enzyme activity with pH changes and exhibited low retention of enzyme activity. At its optimal pH of 7, FF retained only 45% of its enzyme activity after incubation. In contrast, immobilized Flavourzyme, except for those modified with epoxide groups, maintained over 50% of their enzyme activity under optimal pH conditions. As the pH increased, FF's activity dropped substantially to 17.21% of its maximum at pH 10. However, immobilized Flavourzyme retained more than 30% of their initial activity, indicating significantly enhanced resistance to pH variations and improved pH stability.

The thermal stability of free and immobilized Flavourzyme was assessed over a temperature range of 25–75°C, with results depicted in Fig. 5B. After 10 hours at 55°C, FF's activity decreased to 11% of its initial value. In comparison, CHS-F and DHS-F retained over 40% of their activity, while AHS-F and EHS-F retained more than 15%. After 10 hours at 65°C, FF lost almost all its activity, whereas DHS-F still retained 20.65% of its activity, demonstrating strong thermostability. Consistent with the study by Motamedi et al. (Motamedi et al. 2021), which reported that immobilized oxidase on Ni-based magnetic metal-organic framework exhibited greater thermal stability at temperatures ranging from 50 to 70°C compared to free enzymes, the enhanced thermal stability of immobilized Flavourzyme likely arises from interactions between the enzyme and carrier that reduce protein conformational changes at high temperatures.

3.6 Storage stability of immobilized Flavourzyme

Immobilization markedly extends the shelf-life of Flavourzyme (Fig. 6A). FF lost over 99% of its activity within 15 d at 4°C, whereas immobilized preparations retained over 50–90% over the same period. After 55 d, AHS-F retained only 1.26% of residual activity, while CHS-F and DHS-F preserved 41.02% and 51.01%, respectively. EHS-F retained 12.11% of its activity. The enhanced stability is likely attributed to immobilization reducing interactions between enzyme molecules, thereby minimizing aggregation or denaturation (Cavalcante et al. 2021). Enhanced enzyme–carrier contacts, imparted by surface functionalization, provide additional physical protection against thermal and pH-driven denaturation (de Souza et al. 2020), demonstrating that immobilization is an effective strategy to prolong the useful lifetime of Flavourzyme under ambient storage conditions.

3.7 Reusability of immobilized Flavourzyme

Operational stability was assessed over 20 consecutive cycles (Fig. 6B). All immobilized preparations retained over 85% of their initial activity after five cycles and > 55% activity through the 11th cycle. By the conclusion of the 20-cycle experiment, notable variations in residual activity were observed among the different immobilized enzyme systems. Specifically, the residual activities for AHS-F, CHS-F, DHS-F, and EHS-F were measured at 19.22%, 36.15%, 50.26%, and 8.66%, respectively. Compared with single-use FF, immobilization extended the working life 5- to 8-fold, substantially reducing enzyme replacement frequency and operating costs. Notably, DHS-F preserved over 50% activity after 20 cycles, positioning it as a highly promising candidate for enhancing enzyme-catalyzed processes within the food industry.

3.8 Principal component analysis (PCA)

To simplify the interpretation of the complex dataset generated from the evaluation of various immobilized Flavourzyme systems, a PCA model was built to condense the multivariate data set (immobilization rate, enzyme activity recovery, optimal pH/temperature, pH- and thermal-stability, storage stability at 10, 30, and 50 d, and reusability after 10 and 20 cycles) into orthogonal components (Fig. 7). The variables were standardized to ensure equal weighting in the analysis. The first two principal components explained 87.59% of the total variance (PC1 = 68.48%, PC2 = 19.11%; Fig. 7A). PC1 was dominated by positive loadings for storage stability (0.87–0.95), reusability (0.90–0.93) and immobilization rate (0.75), identifying this axis as a “stability–capacity” factor. PC2 was primarily influenced by optimal temperature (0.74) and pH-stability at pH 7 (0.54), with minor contributions from storage-50 d (0.46) and reusability-20 cycles (0.31), and can be interpreted as a “temperature–pH robustness” factor.

The score plot (Fig. 7B) visualizes the distribution of different immobilized Flavourzyme samples across the two principal components. FF is located in the negative PC1/positive PC2 quadrant, reflecting poor stability but high temperature optimum. CHS-F and DHS-F cluster on the positive PC1 side, with DHS-F exhibiting the highest PC2 score, indicating the best combination of long-term stability and temperature–pH tolerance. AHS-F and EHS-F fall in the negative PC1 space, consistent with their relatively lower storage and recycling performance.

Thus, PCA provided insights into the relationships among various properties of the immobilized Flavourzyme systems, highlighting the importance of storage stability and reusability in differentiating their performance. The distinct clustering of immobilized systems based on their PCA scores indicates that different immobilization strategies result in systems with unique performance profiles. Specifically, DHS-F and CHS-F performed well on variables such as Storage stability and Reusability, making them suitable for applications requiring high stability and repeat use. These findings can guide future research and development efforts towards optimizing immobilization processes for specific industrial applications.

4. Conclusion

This study systematically investigated the surface modification of hydrated silica and its application in Flavourzyme immobilization, aligning with sustainable practices advocated by the food industry. Utilizing DR-FTIR and XPS, we characterized various modified carriers and systematically evaluated their impact on enzyme immobilization efficiency and properties. Our findings underscored the capacity of surface modifications to enhance enzyme loading capacity and modulate enzymatic properties, thereby offering a promising approach to improve the sustainability of biocatalytic processes. Through single-factor experiments, we identified the optimal immobilization conditions for each modified carrier, leading to immobilized enzyme systems that demonstrated significant improvements in catalytic performance. Notably, the optimal pH and temperature for these systems shifted compared to their free enzyme counterparts, reflecting the influence of the carrier modifications on enzymatic activity. Moreover, the immobilized enzymes exhibited enhanced stability across a range of pH conditions and elevated temperatures, which is crucial for their application in industrial settings where conditions can vary widely. Storage and reusability tests further underscored the practical applicability of the immobilized enzyme systems. PCA confirmed that storage stability and reusability are the principal discriminators of performance, with DHS-F offering the best compromise between robustness and recyclability. Collectively, these results provide valuable insights for the development of efficient and robust enzyme immobilization systems, contributing to cleaner production practices and sustainable industrial applications.

Declarations

Declaration of competing interest

The authors declare that they have no known competing financial interests or personal relationships that could have appeared to influence the work reported in this paper.

Funding

This work was supported by the Guangdong province general colleges and universities characteristic innovation category project (2021KTSCX003) and Shandong province science and technology-based small and medium-sized enterprises innovation ability enhancement project mission statement (2022TSGC2558).

Author Contribution

Xu Zhao drafted the work and revised it critically for important intellectual content;Xu Zhao, Yuqin Cheng and Lei Cai made substantial contributions to the conception or design of the work and the acquisition, analysis, and interpretation of data;Cui Chun approved the version to be published; and agree to be

accountable for all aspects of the work in ensuring that questions related to the accuracy or integrity of any part of the work are appropriately investigated and resolved.

Data availability

The data that support the findings of this study are available from the corresponding author upon reasonable request.

References

1. Ashkan, Z., Hemmati, R., Homaei, A., Dinari, A., Jamlidoost, M., & Tashakor, A. (2021). Immobilization of enzymes on nanoinorganic support materials: An update. *International Journal of Biological Macromolecules*, *168*, 708–721.
2. Atrei, A., Chokheli, S., Corsini, M., Jozsef, T., & Di Florio, G. (2024). Uptake of Magnetite Nanoparticles on Polydopamine Films Deposited on Gold Surfaces: A Study by AFM and XPS. Nanomaterials. 14(21).
3. Benke, M. B., Mermut, A. R., & Chatson, B. (1998). Carbon-13 CP/MAS NMR and DR-FTIR spectroscopic studies of sugarcane distillery waste. *Canadian Journal of Soil Science*, *78*(1), 227–236.
4. Bhatia, L., Jha, H., Sarkar, T., & Sarangi, P. K. (2023). Food Waste Utilization for Reducing Carbon Footprints towards Sustainable and Cleaner Environment: A Review. *International Journal of Environmental Research and Public Health* 20(3).
5. Bolivar, J. M., & Nidetzky, B. (2019). The Microenvironment in Immobilized Enzymes: Methods of Characterization and Its Role in Determining Enzyme Performance. *Molecules* 24(19).
6. Cai, A., Zhang, Q. C., Hou, F., Li, G. Z., Xi, S. B., Fan, X. B., Peng, W. C., & Li, Y. (2025). Fine-tuning coordination from W-O to W-N in graphene gel based single-atom W for hydrogenation of *p*-chloronitrobenzene. *Aiche Journal* 71(6).
7. Carballares, D., Rocha-Martin, J., & Fernandez-Lafuente, R. (2022). Chemical amination of immobilized enzymes for enzyme coimmobilization: Reuse of the most stable immobilized and modified enzyme. *International Journal of Biological Macromolecules*, *208*, 688–697.
8. Cavalcante, F. T. T., Cavalcante, A. L. G., de Sousa, I. G., Neto, F. S., & dos Santos, J. C. S. (2021). Current Status and Future Perspectives of Supports and Protocols for Enzyme Immobilization. Catalysts. 11(10).
9. Chao, C., Zhang, B., Zhai, R., Xiang, X., Liu, J. D., & Chen, R. F. (2014). Natural Nanotube-Based Biomimetic Porous Microspheres for Significantly Enhanced Biomolecule Immobilization. *Acs Sustainable Chemistry & Engineering*, *2*(3), 396–403.
10. Chen, Y., Eder, S., Schubert, S., Gorgerat, S., Boschet, E., Baltensperger, L., Boschet, E., Städeli, C., Kuster, S., Fischer, P., & Windhab, E. J. (2021). Influence of Amylase Addition on Bread Quality and

Bread Staling. *ACS Food Science & Technology*, *1*(6), 1143–1150.

11. Das, B., Kundu, R., & Chakravarty, S. (2022). Preparation and characterization of graphene oxide from coal. *Materials Chemistry and Physics*. 290.
12. Daulay, A., Astuti, W., Mufakhir, F. R., Prasetia, H., & Samada, L. H. (2024). Chitosan grafted alginate and polyvinylpyrrolidone as the binder for porous silicon nanoparticles from coal fly ash in lithium-ion batteries. *Journal of Electroanalytical Chemistry*. 952.
13. De Meutter, J., & Goormaghtigh, E. (2021). Amino acid side chain contribution to protein FTIR spectra: impact on secondary structure evaluation. *European Biophysics Journal with Biophysics Letters*, *50*(3–4), 641–651.
14. de Souza, T. C., Fonseca, T. D., Silva, J. D., Lima, P. J. M., Neto, C., Monteiro, R. R. C., Rocha, M. V. P., de Mattos, M. C., dos Santos, J. C. S., & Gonçalves, L. R. B. (2020). Modulation of lipase B from *Candida antarctica* properties via covalent immobilization on eco-friendly support for enzymatic kinetic resolution of *rac*-indanyl acetate. *Bioprocess and Biosystems Engineering*, *43*(12), 2253–2268.
15. Dotsenko, A., Sinelnikov, I., Zorov, I., Denisenko, Y., Rozhkova, A., & Shcherbakova, L. (2024). The Protein Engineering of Zearalenone Hydrolase Results in a Shift in the pH Optimum of the Relative Activity of the Enzyme. *Toxins* 16(12).
16. Eshaghi, A., & Pouransari, Z. (2025). Optimizing Arrhenius parameters for multi-step reactions via metaheuristic algorithms. *Journal of Mathematical Chemistry*, *63*(4), 1065–1092.
17. Feng, L., Qiao, Y., Zou, Y. F., Huang, M., Kang, Z. L., & Zhou, G. H. (2014). Effect of Flavourzyme on proteolysis, antioxidant capacity and sensory attributes of Chinese sausage. *Meat Science*, *98*(1), 34–40.
18. Flores, E. E. E., Cardoso, F. D., Siqueira, L. B., Ricardi, N. C., Costa, T. H., Rodrigues, R. C., Klein, M. P., & Hertz, P. F. (2019). Influence of reaction parameters in the polymerization between genipin and chitosan for enzyme immobilization. *Process Biochemistry*, *84*, 73–80.
19. Fujisaki, S., Yamaguchi, Y., Kobayashi, H., Shinoda, K., Yamada, M., Kawamura, K., & Izawa, M. (2024). Oxidation state of cobalt oxide in thermal-cyclic atomic layer etching of cobalt by plasma oxidation and organometallization. *Aip Advances* 14(4).
20. Gao, P., Su, Y. L., Zhang, W. Y., Pang, X. Y., Xie, N., Zhang, M., Lv, J. P., & Zhang, S. W. (2022). Chemical and Flavor Characteristics of Enzyme-Modified Cheese Made by Two-Stage Processing. *Gels* 8(3).
21. Gennari, A., Mobayed, F. H., Rafael, R. D., Rodrigues, R. C., Sperotto, R. A., Volpato, G., & de Souza, C. F. V. (2018). Modification of Immobead 150 Support for Protein Immobilization: Effects on the Properties of Immobilized *Aspergillus oryzae* β-Galactosidase. *Biotechnology Progress*, *34*(4), 934–943.
22. Grossmann, K. K., Merz, M., Appel, D., Thaler, T., & Fischer, L. (2021). Impact of Peptidase Activities on Plant Protein Hydrolysates Regarding Bitter and Umami Taste. *Journal of Agricultural and Food Chemistry*, *69*(1), 368–376.

23. Guisan, J. M., Fernandez-Lorente, G., Rocha-Martin, J., & Moreno-Gamero, D. (2022). Enzyme immobilization strategies for the design of robust and efficient biocatalysts. *Current Opinion in Green and Sustainable Chemistry*. 35.
24. Guo, W. J., Ding, W. J., Yao, Y. Q., Rajca, S., Li, Q. L., Jiang, H., Rajca, A., & Wang, Y. (2023). Aromatic C-C Bond Cleavage in a Curved π-System of Aminocorannulene. *Organic Letters*, *25*(21), 3972–3977.
25. Haghighat-Kharazi, S., Kasaai, M. R., Milani, J. M., & Khajeh, K. (2020). Antistaling properties of encapsulated maltogenic amylase in gluten-free bread. *Food Science & Nutrition*, *8*(11), 5888–5897.
26. Huang, Z. J., Huang, Z. Y., Feng, L. J., Luo, X. W., Wu, P. X., Cui, L. H., & Mao, X. Y. (2018). Modified cellulose by polyethyleneimine and ethylenediamine with induced Cu(II) and Pb(II) adsorption potentialities. *Carbohydrate Polymers*, *202*, 470–478.
27. Intarabumrung, W., Kuntharin, S., Harnchana, V., Prada, T., Kasemsiri, P., Hunt, A. J., & Supanchaiyamat, N. (2022). Facile Synthesis of Biobased Polyamide Derived from Epoxidized Soybean Oil as a High-Efficiency Triboelectric Nanogenerator. *Acs Sustainable Chemistry & Engineering*, *10*(41), 13680–13691.
28. Jiang, J-H., Zhu, L-P., Li, X-L., Xu, Y-Y., & Zhu, B-K. (2010). Surface modification of PE porous membranes based on the strong adhesion of polydopamine and covalent immobilization of heparin. *Journal of Membrane Science*, *364*(1), 194–202.
29. Johansson, B. L., Belew, M., Eriksson, S., Glad, G., Lind, O., Maloisel, J. L., & Norrman, N. (2003). Preparation and characterization of prototypes for multi-modal separation aimed for capture of positively charged biomolecules at high-salt conditions. *Journal of Chromatography A*, *1016*(1), 35–49.
30. Katic, K., Banjanac, K., Simovic, M., Corovic, M., Milivojevic, A., Marinkovic, A., & Bezbradica, D. (2021). Development of protease nanobiocatalysts and their application in hydrolysis of sunflower meal protein isolate. *International Journal of Food Science and Technology*, *56*(9), 4287–4297.
31. Laguri, C., Silipo, A., Martorana, A. M., Schanda, P., Marchetti, R., Polissi, A., Molinaro, A., & Simorre, J. P. (2018). Solid State NMR Studies of Intact Lipopolysaccharide Endotoxin. *Acs Chemical Biology*, *13*(8), 2106–2113.
32. Li, D. M., Mei, L., Ding, X. G., & Zhou, D. (2024). Preparation of highly stable immobilized *Candida antarctica* lipase B (CALB) through adjusting the surface properties of carrier: Preparation, characterization and performance evaluation. *International Journal of Biological Macromolecules*. 280.
33. Li, Q., Chang, B. Y., Huang, G., Wang, D., Gao, Y., Fan, Z. J., Sun, H. B., & Sui, X. N. (2025). Differential Enzymatic Hydrolysis: A Study on Its Impact on Soy Protein Structure, Function, and Soy Milk Powder Properties. Foods. 14(5).
34. Li, R., Zhang, Z. H., Pei, X. M., & Xia, X. L. (2020). Covalent Immobilization of L-Asparaginase and Optimization of Its Enzyme Reactor for Reducing Acrylamide Formation in a Heated Food Model System. *Frontiers in Bioengineering and Biotechnology*. 8.

35. Li, Y. C., Li, Y. X., Feng, X., Chai, Y. M., & Liu, C. G. (2018). Adsorptive Removal of Acetaldehyde from Propylene Oxide Produced by the Hydrogen Peroxide to Propylene Oxide Process. *Acs Omega*, *3*(11), 15272–15280.
36. Maghraby, Y. R., El-Shabasy, R. M., Ibrahim, A. H., & Azzazy, H. M. E. (2023). *Enzyme Immobilization Technologies and Industrial Applications*. Acs Omega.
37. Mao, S. C., Jiang, J. W., Xiong, K., Chen, Y. Q., Yao, Y. Y., Liu, L. C., Liu, H. B., & Li, X. (2024). Enzyme Engineering: Performance Optimization, Novel Sources, and Applications in the Food Industry. Foods. 13(23).
38. Mohamad, N. R., Marzuki, N. H. C., Buang, N. A., Huyop, F., & Wahab, R. A. (2015). An overview of technologies for immobilization of enzymes and surface analysis techniques for immobilized enzymes. *Biotechnology & Biotechnological Equipment*, *29*(2), 205–220.
39. Motamedi, N., Barani, M., Lohrasbi-Nejad, A., Mortazavi, M., Riahi-Medvar, A., Varma, R. S., & Torkzadeh-Mahani, M. (2021). Enhancement of Thermostability of *Aspergillus flavus* Urate Oxidase by Immobilization on the Ni-Based Magnetic Metal-Organic Framework. Nanomaterials. 11(7).
40. Nasiri, A., Ghollasi, M., Eskandari, K., & Darvishi, E. (2025). Immobilization of lipase enzyme onto herbal silver nanoparticles and examination of biochemical parameters of immobilized enzyme. *Brazilian Journal of Chemical Engineering*, *42*(2), 443–454.
41. Nowak, J. K., Dybska, E., Dworacka, M., Tsikhan, N., Kononets, V., Bermagambetova, S., & Walkowiak, J. (2021). Ileal Lactase Expression Associates with Lactase Persistence Genotypes. *Nutrients* 13(4).
42. Patel, V. B., Chatterjee, S., & Dhoble, A. S. (2022). A review on pectinase properties, application in juice clarification, and membranes as immobilization support. *Journal of Food Science*, *87*(8), 3338–3354.
43. Saroja, A., & Bhat, B. R. (2021). Cobalt Schiff Base Immobilized on Graphene Nanosheet with N, O linkage for Cross-Coupling Reaction (vol 58, pg 590, 2019). Industrial & Engineering Chemistry Research. 60(45), 16543–16543.
44. Shen, Y. R., Jiang, P. P., Wang, Y. C., Bian, G., Wai, P. T., & Dong, Y. M. (2018). MoO < sub>3@SiO < sub>2 nanoreactors: Synthesis with a thermal decomposition strategy and catalysis on alkenes epoxidation. *Journal of Solid State Chemistry*, *264*, 156–164.
45. Shuai, X. X., Gao, L. Z., Geng, Q., Li, T., He, X. M., Chen, J., Liu, C. M., & Dai, T. T. (2022). Effects of Moderate Enzymatic Hydrolysis on Structure and Functional Properties of Pea Protein. Foods. 11(15).
46. Tadesse, M., & Liu, Y. (2025). Recent Advances in Enzyme Immobilization: The Role of Artificial Intelligence, Novel Nanomaterials, and Dynamic Carrier Systems. *Catalysts* 15(6).
47. Talik, P., Moskal, P., Proniewicz, L. M., & Weselucha-Birczynska, A. (2020). The Raman spectroscopy approach to the study of Water-Polymer interactions in hydrated hydroxypropyl cellulose (HPC). *Journal of Molecular Structure*. 1210.
48. Tan, L. P., Liu, T., Zhang, Y. M., Xue, N. N., & Hu, P. C. (2023). Enhance selective separation of vanadium and iron from acid-leaching solution with sulfamic acid modified resin. *Chemical*

Engineering Journal. 457.

49. Tang, W., Chen, C., Sun, W., Wang, P., & Wei, D. Z. (2019). Low-cost mussel inspired poly(Catechol/Polyamine) modified magnetic nanoparticles as a versatile platform for enhanced activity of immobilized enzyme. *International Journal of Biological Macromolecules*, *128*, 814–824.
50. Wiltschi, B., Cernava, T., Dennig, A., Casas, M. G., Geier, M., Gruber, S., Haberbauer, M., Heidinger, P., Acero, E. H., Kratzer, R., Luley-Goedl, C., Müller, C. A., Pitzer, J., Ribitsch, D., Sauer, M., Schmölzer, K., Schnitzhofer, W., Sensen, C. W., Soh, J., Steiner, K., Winkler, C. K., Winkler, M., & Wriessnegger, T. (2020). Enzymes revolutionize the bioproduction of value-added compounds: From enzyme discovery to special applications. *Biotechnology Advances*. 40.
51. Yang, J., Jiang, C. C., Bao, R. Q., Liu, M. Y., Lv, J., Yang, Z. X., Xu, W. H., Liang, H. P., Ji, C. F., Li, S. J., Zhang, S. F., & Lin, X. P. (2020). Effects of flavourzyme addition on physicochemical properties, volatile compound components and microbial community succession of *Suanzhayu*. *International Journal of Food Microbiology*. 334.
52. Yang, Q., Wang, B. C., Zhang, Z., Lou, D. S., Tan, J., & Zhu, L. C. (2017). The effects of macromolecular crowding and surface charge on the properties of an immobilized enzyme: activity, thermal stability, catalytic efficiency and reusability. *Rsc Advances*, *7*(60), 38028–38036.
53. Yang, W. H., Lu, F. P., & Liu, Y. H. (2023). Recent Advances of Enzymes in the Food Industry. *Foods* 12(24).
54. Zdarta, J., Meyer, A. S., Jesionowski, T., & Pinelo, M. (2018). A General Overview of Support Materials for Enzyme Immobilization: Characteristics, Properties, Practical Utility. *Catalysts* 8(2).
55. Zhang, S. Y., Zhang, C. Y., Qiao, Y., Xing, L. J., Kang, D. C., Khan, I. A., Huang, M., & Zhou, G. H. (2017). Effect of Flavourzyme on proteolysis, antioxidant activity and sensory qualities of Cantonese bacon. *Food Chemistry*, *237*, 779–785.
56. Zhao, X., Cheng, Y. Q., Xu, J. C., & Cui, C. (2025). Dopamine-modified hydrated silica immobilized Flavourzyme for efficient bioactive peptide release from (β-lactoglobulin. *Food Chemistry*. 487.
57. Zhao, Y. C., Yu, D. L., Zhou, H. W., Tian, Y. J., & Yanagisawa, O. (2005). Turbostratic carbon nitride prepared by pyrolysis of melamine. *Journal of Materials Science*, *40*(9–10), 2645–2647.
58. Zheng, X. Y., Li, Q., Tian, J., Zhan, H. L., Yu, C., Wang, S. J., & Sun, X. T. (2021). Novel Strategy of Mussel-Inspired Immobilization of Naringinase with High Activity Using a Polyethylenimine/Dopamine Co-deposition Method. *Acs Omega*, *6*(4), 3267–3277.

Figures

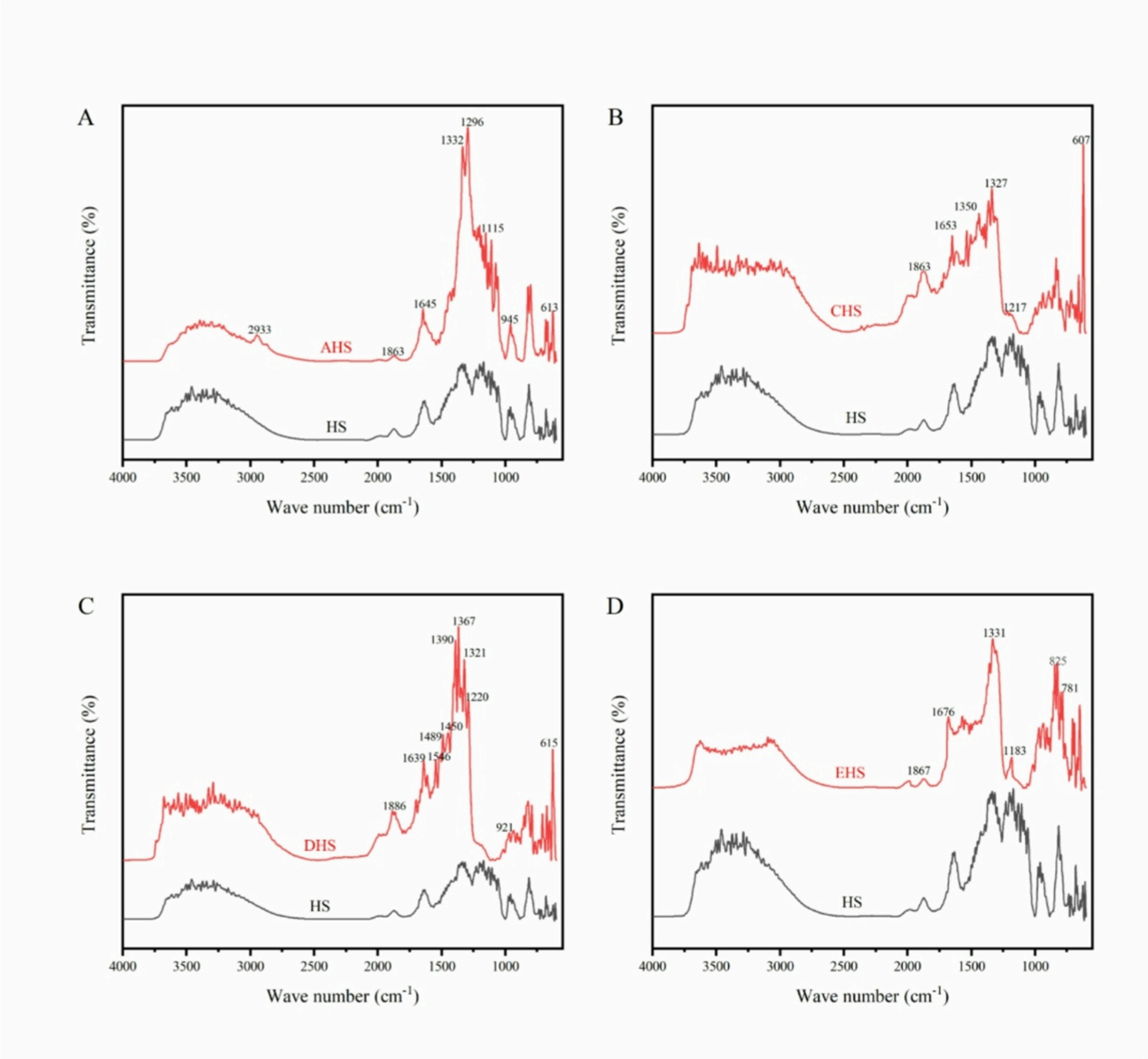


Figure 1

DR-FTIR spectra of pristine and surface-functionalized hydrated silica (HS, pristine hydrated silica; AHS, amino-modified hydrated silica; CHS, carboxyl-modified hydrated silica; DHS, dopamine-modified hydrated silica; EHS, epoxy-modified hydrated silica).

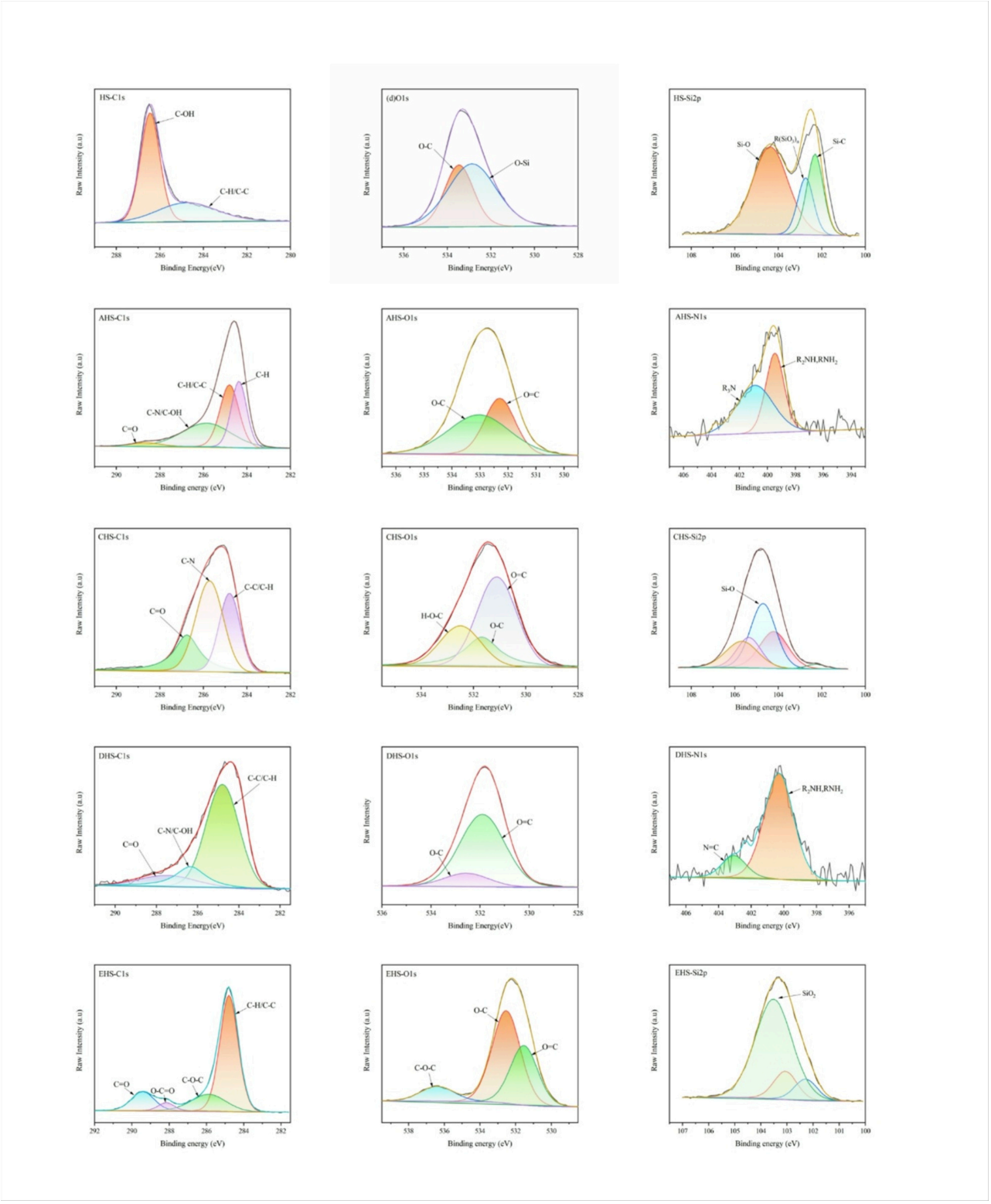


Figure 2

XPS survey and high-resolution (C 1s, O 1s, N 1s, Si 2p) spectra of hydrated silica before and after modification.

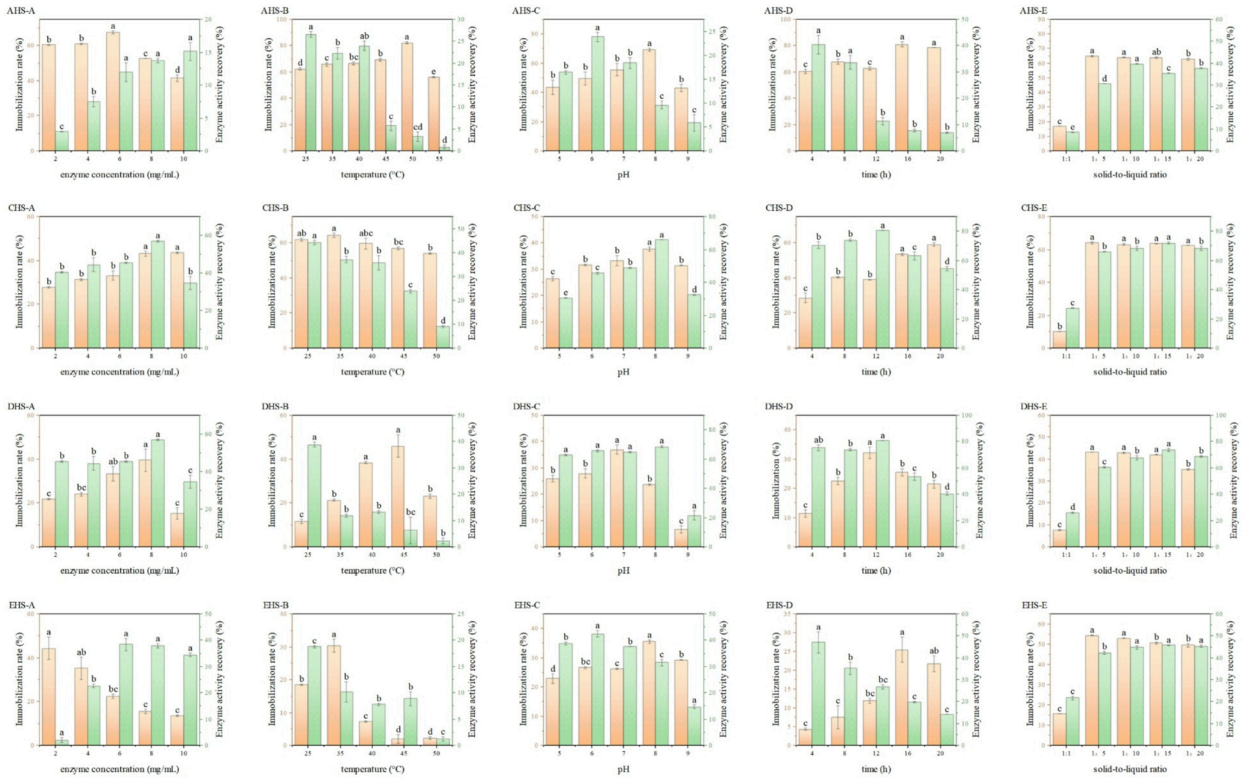


Figure 3

Optimization of Flavourzyme immobilization on various modified hydrated silica carriers.

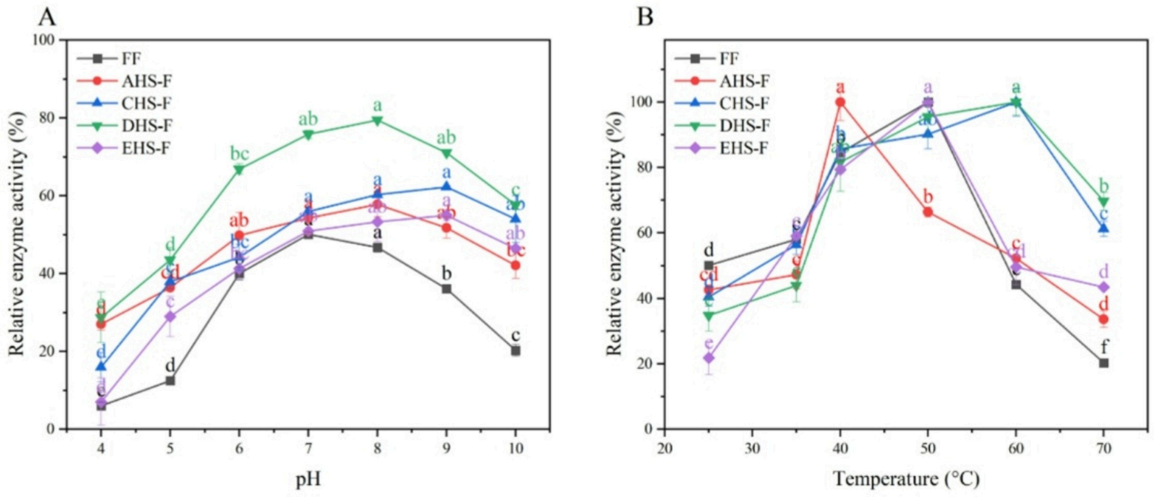


Figure 4

Optimal catalytic pH (A) and temperature (B) of free and immobilized Flavourzyme.

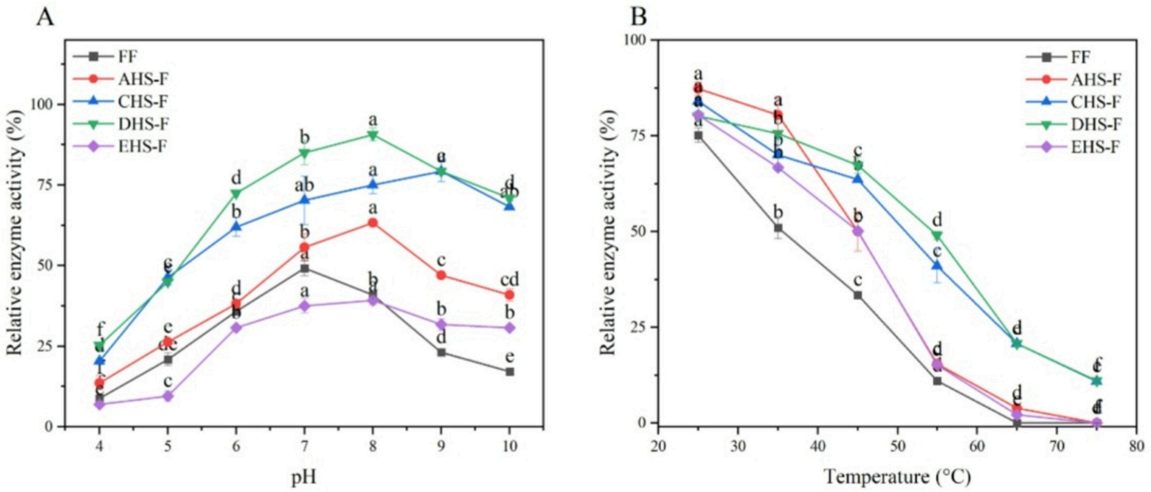


Figure 5

Acid-base (A) and thermal (B) stability of free and immobilized Flavourzyme.

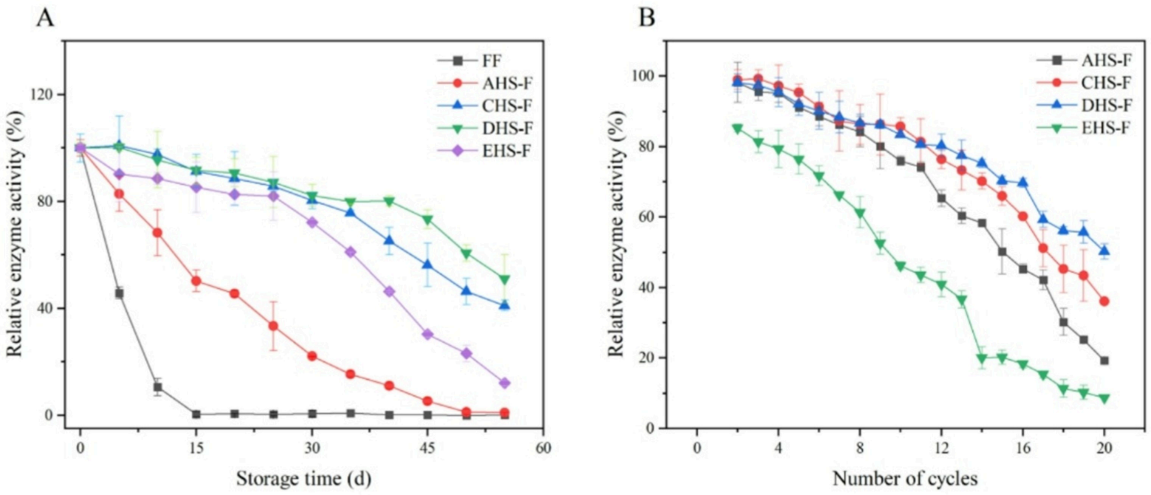


Figure 6

Storage stability (A) and reusability (B) of immobilized Flavourzyme.

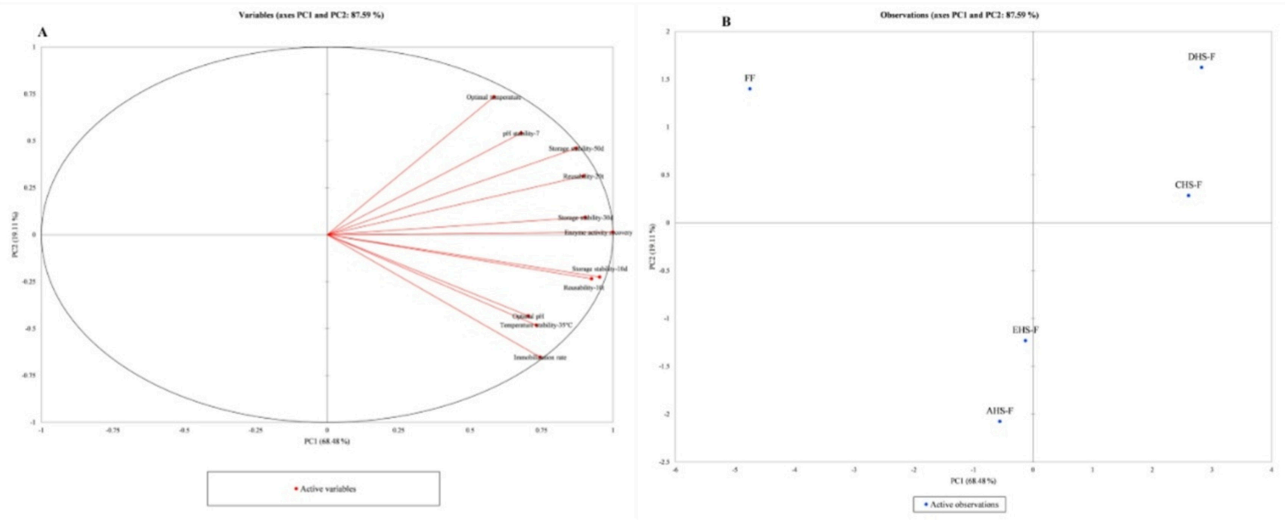


Figure 7

Principal component analysis (PCA, A) and scores (B) of immobilized Flavourzyme.